Spatial Distribution of Canopy Gaps in Lodgepole Pine Forest

RAE MELLOH[1] , JERRY BALLARD[2], JANET HARDY[1], CURTIS WOODCOCK[3],
J. LIU[3], JIM SMITH[4], GEOFF KOENIG[1], AND ROBERT DAVIS[1]

ABSTRACT

Forest canopy, through its influence on optical, infrared, and microwave signatures observed from remote sensing platforms, impacts the retrieval of information on snow cover properties and extent. The number and size of gaps within and between tree crowns determines the scale and quality of information that can be obtained remotely. This paper explores ground based descriptions of the spatial distribution of canopy gaps using hemispherical photography and summarizes how the statistics may be useful in validating 1) a synthetic 3-D canopy to be used in an infrared canopy model, and 2) a terrain capable, viewable gap fraction model. Hemispherical photographs were taken with a Nikkor 8mm/f2 lens at 20-m grid spacing in the Fraser Experimental Forest, an area of predominantly lodgepole pine (*Pinus contorta*), and were analyzed with Gap Light Analyzer software. The study site is part of the ongoing interagency Cold Lands Processes Experiment (CLPX) that seeks to advance techniques for large scale remote observation of hydrologic properties (Cline et al 2002). Gap fraction distributions, gap fraction variograms, and subcanopy radiation environment were characterized for the site. Gap fraction distributions for discontinuous canopy had broader peaks than for continuous canopy, reflecting the greater heterogeneity in discontinuous settings. Mean correlation lengths in continuous settings increased from 10^o to 20^o in azimuth between 30^o and 60^o zeniths and the maximum variances also consistently increased. In comparison, discontinuous setting correlation lengths were longer but the trend with zenith angle was less consistent. Total daily solar radiation transmittance varied sensitively with location within the site, providing addition characterizations for comparisons between actual and modeled canopy.

Keywords: spatial distribution, canopy models, lodgepole pine, gap fractions

INTRODUCTION

One of the objectives of the Cold Land Processes Experiment (CLPX) is to advance techniques for large-scale observation of hydrologic properties, including water storage and freeze-thaw state (Cline et al 2002). The number, arrangement, and size of gaps within and between tree crowns determine the amount of snow that can be viewed in a forested scene. Gap characteristics influence the optical, infrared and radiative environment within the forest, and influence the remotely sensed signatures in these wavelengths. Viewable gap fractions in forested terrain are dependent on the slope, aspect and viewing angle, as well as stand structure, crown geometry and foliage density (Liu and Woodcock 2002).

[1]ERDC-CRREL, 72 Lyme Rd., Hanover, New Hampshire 03773-1290 USA
[2]ERDC –Environmental Laboratory, 3909 Halls Ferry Road, Vicksburg, MS 39180-6199
[3]Department of Geography, Boston University, 675 Commonwealth Avenue, Boston, MA 02215
[4]NASA Goddard Space Flight Center, Greenbelt, MD USA.

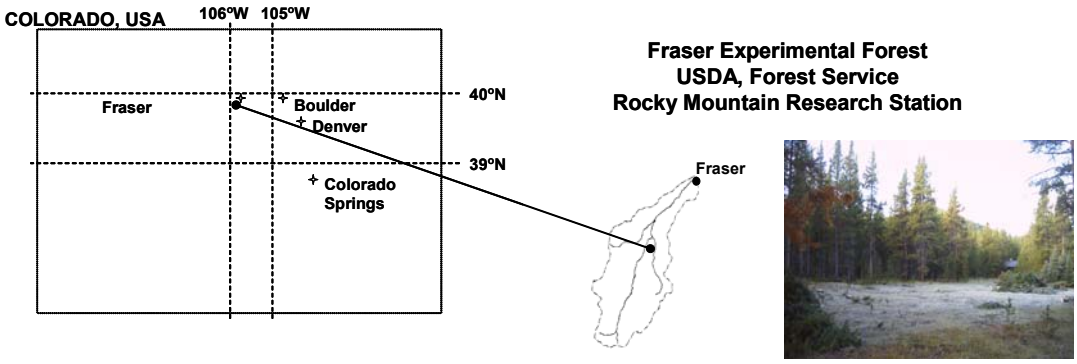

Figure 1. Location of the Fraser LSOS within the St. Louis Creek drainage basin in the Fraser Experimental Forest, USDA, Rocky Mountain Research Station.

The study site is a managed forest within the Fraser Experimental Forest of the USDA Forest Service, Rocky Mountain Research Station near Fraser, Colorado (39º54'13"N, 105º53'00"W) at 2760-m elevation (Fig. 1), referred to in the CLPX as the Local Scale Observation Site (LSOS). The site is a triangular area (120-m on a side) of predominantly lodgepole pine (*Pinus contorta*) and includes a central opening.

This paper explores ground based canopy gap descriptions extracted from hemispherical photographs for use in validating two canopy models that are in the developmental stage. In the process of doing this, the gap environment of the LSOS was characterized. The purpose of the first model is infrared scene simulation (Koenig et al. 2000). The model uses a synthesized three-dimensional (3-D) canopy to populate a voxel mesh representation of the forest. Each element represents a homogeneous part of the forest (needles, branches, wood, ground, etc.), as described by Kimes and Kirchner (1982). A geometric representation of the composed 3-D scene was used to derive synthetic hemispherical images to compare with actual hemispherical images. Comparisons explored include gap fraction distributions, gap spatial dependence, and spatial variation of solar radiation transmittance. The second model is a terrain-capable version (Liu and Woodcock 2002) of the hybrid Geometric Optical Radiative Transfer model (Li et al. 1995) called VGF (viewable gap fraction). VGF was demonstrated here to illustrate the importance of considering terrain aspect and slope in the extraction of snowcover information from remotely sensed scenes. The area used for the VGF demonstration was the Fraser, Colorado USGS 7.5 minute topographic quadrangle.

MEASUREMENTS AND OBSERVATIONS

Tree Location and Crown Geometry

A 10-m resolution grid was established over the triangular plot using a transit level, compass and measuring tape. A total of 77, 10- by 10-m cells were marked off with a combination of wooden stakes and temporary wire flags. The locations of the grid corner points agreed within 20-cm when cross-checked during grid layout. Tree locations and crown geometery were measured for representative areas of continuous and discontinuous canopy portions of the plot. The continuous portion of the plot was uniformly dense and the discontinuous portion included the small central opening and the edge of the opening. The x, y locations of tree trunks were measured by first positioning measuring tapes along two sides of the 10-m cells. Two observers sighted a tree directly between them, making minor adjustments in their stance along the tapes until their x-distances agreed at 10-cm resolution. The y-distances to the trees were measured using an Impulse laser rangefinder (range accuracy of 0.03-m at 50-m distance). The x-y locations were plotted on grid paper and later digitized to create a map. To date, tree locations have not been mapped in 14 of the cells. Diameters of the tree trunks (DBH) were measured at 1.3-m

height using a flexible tape. Maximum crown widths were measured with a tape pulled between the two observers. Tree crown heights, bottom and top, were measured with the laser range finder. Crown heights and DBH were actual measures in only twelve of the cells. In the remaining 65 cells, unique crown heights were not recorded but each tree was assigned to one of 30 index forms of approximate similar dimension.

Detailed Geometric Tree Measurements

Trees selected for detailed measurements included four large and two juvenile lodgepole pines. Geometric properties of these representative trees were measured by tape and protractor. The measurements included trunk diameter at multiple heights, main branch length, second and third order branch length, needle length, needle width, number of needles per needle cluster, twig length, twig diameter, crown shape, crown bottom height, and crown height.

Collecting Hemispherical Photographs

Hemispherical photographs were taken over the grid at a staggered 20-m interval (Fig. 2) with a Nikkor 8-mm f/2.8 hemispherical lens (180^o field of view) with integral red filter. The lens was mounted on a Nikon FM2 35-mm camera body with data back for recording print numbers on the film. The camera was mounted on a tripod at approximately 1-m height and leveled with a bubble level. The photographs were taken over a period of several days in early November 2001 during which sky conditions were clear. Photographs were taken at dusk and dawn to avoid light reflections of direct sunlight from the canopy that could be confused with sky. The top of the camera was oriented north by approximate alignment along the flagged transect lines. Black and white TMAX 400 ASA film was used and three exposures were taken, including the correct exposure, and plus and minus half-stops. The self-timer release was used to minimize camera movement. The wind was calm, minimizing canopy movement. The negatives were digitized with a Noritzu scanner to 1024 vertical by 1536 horizontal pixels, resulting in 1020 pixels across the hemisphere diameter. Distortion in the digitization process has not been determined yet, but is expected to be minor. The correct exposure images were chosen for analysis and a consistent threshold level of 128 DN (digital number) was used to separate sky and canopy. The center and diameter of the hemisphere on the photo-images must be known in order to register the image with the hemispherical analysis grid. The diameter was established by taking a photograph in which the outer edge of the hemisphere could be readily identified. A photograph taken with the camera set between light colored buildings was used to do this. The hemisphere center was set consistently on each photo-image by using a set distance from the print number.

Gap Fraction Frequency Distributions

Zenith angles versus gap fractions were plotted for each hemispherical photo-image, and the plots were grouped by continuous and discontinuous canopy settings (Fig. 3). The gap fractions were determined with Gap Light Analyzer image analysis software (Fraser et al. 1999) using a hemispherical grid overlay with 4^o azimuth and 2^o zenith grid resolution. Gap fraction frequency plots (Fig. 4) were developed from the data shown in Figure 3, for the nine zenith angle ranges (0^o to 10^o, 10^o to 20^o, etc.).

Gap Fraction Correlation Lengths

The spatial dependencies of gap fractions for the continuous and discontinuous settings were examined for zenith view angles of 30 ^{o}, 40^o, 50^o and 60^o. This range encompasses the zone of most significant direct radiation penetration during the 2002 CLPX intensive observation periods (IOPs) of 16-24 February and 22-31 March (Melloh et al 2002). The semi-variograms (γ) were calculated for each lag distance (h) measured in angular degrees in azimuth as

$$\gamma(h) = \frac{1}{2(N-h)} \sum_{i=1}^{N-h} \left[z_i - z_{(i+h)} \right]^2 \qquad (1)$$

where N-h is the number of pair comparisons of the series values (z_1, z_2, z_3, etc.) (Webster and Oliver 2001). Canopy elements close to one another tend to have similar gap fractions compared to elements further apart. The small variance at shorter lags and increasingly larger variance at longer lags results in the characteristic variogram shape (Fig. 5). The angular distance over which the canopy elements are spatially dependent, is referred to as the correlation length, and is equivalent to the lag distance at which the variance levels-off to a "sill" of maximum variance. The resulting variograms for each photo-image (Fig. 5a) were averaged to find mean variograms for the 30^o, 40^o, 50^o and 60^o zenith view angles (Fig.5b).

Canopy Transmittance and Plant Area Index

A number of opportunities exist to compare the light environment below the canopy using actual and synthetic hemispherical images. Several will be discussed, but only the total daily radiation transmittance (Fig. 6) will be shown in map form. The map of total daily radiation transmittance was developed for 16-24 February by accounting for both diffuse and direct radiation. The simplified radiation model within GLA assumes that when the sun position is obstructed by canopy the direct radiation is zero and when unobstructed is equal to the above canopy value (Fraser et al. 1999). Beam enrichment due to scattered and reflected radiation is not included. Diffuse radiation calculations assumed all regions of the sky hemisphere were equally

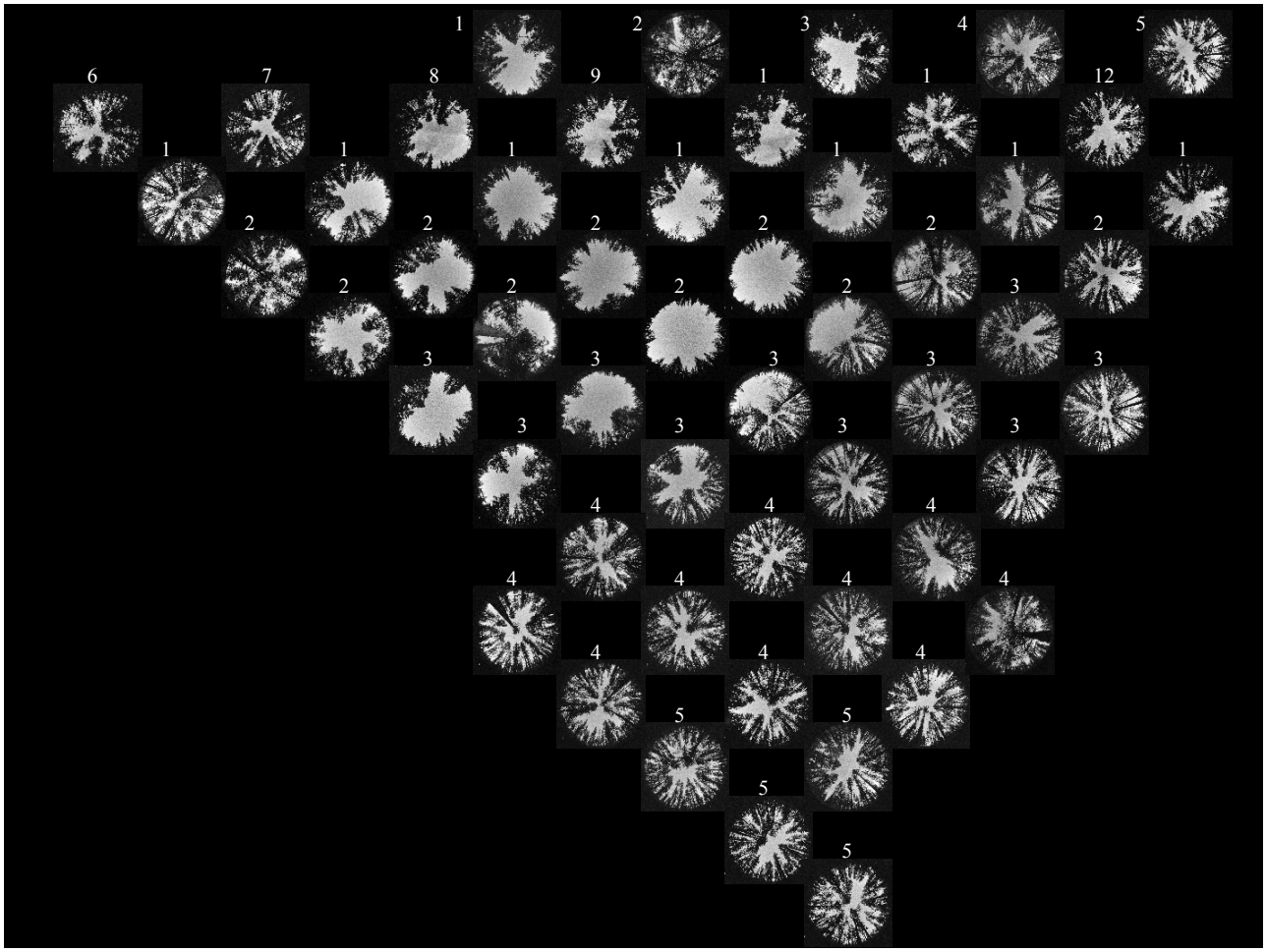

Figure 2. Hemispherical photographs taken with a Nikkor 8mm/F2 lens at staggered 20-m spacing. Photographs 1,3,8-10,14-17,21-23,26-29,31-33, 36, and 37 are discontinuous, and the remainder, continuous canopy settings.

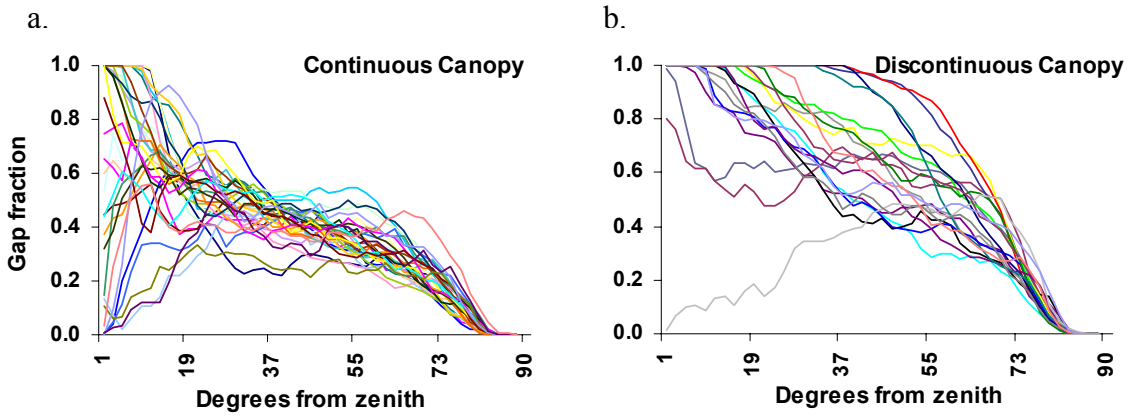

Figure 3. Gap fraction versus zenith angle curves for a) the continuous, and b) discontinuous settings. The 90° zenith is near the horizon and 0° zenith is directly overhead (sky). The high variation in gap fractions near 0° reflect that some locations have tree crowns directly overhead while others do not.

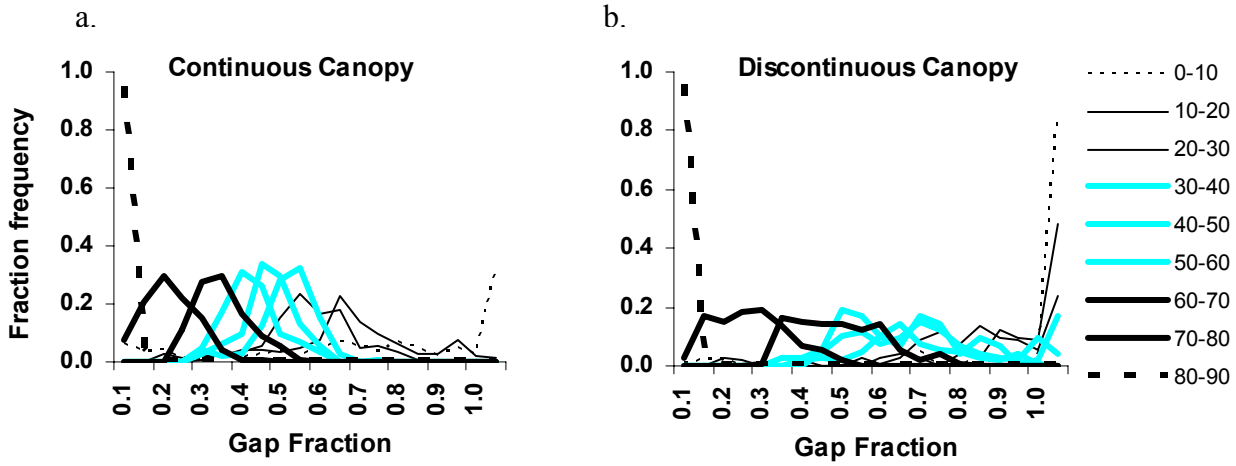

Figure 4. Gap fraction versus zenith angle frequency curves for a) the continuous, and b) discontinuous settings. The fine lines are skyward (0° to 30° zenith) and include the taller tree crowns, the mid-weight lines represent the main canopy (30° to 60°), and the heavy lines (60° to 90° zenith) include low canopy.

bright according to the Universal Overcast Sky (UOC) model (Hutchinson et al., 1980) and that unobstructed sky regions contributed diffuse radiation. A cloudiness index was set at 0.5 and permitted half the extraterrestrial radiation through the atmosphere. Other assumptions were that the fraction of visible radiation (400-700-nm) was 0.5, a beam fraction of 0.5 assigned half the radiation as diffuse, and the solar constant was 1367 Wm^{-2}. GLA computes LAI (leaf area index) with a linear averaging algorithm (Welles and Norman 1991) based on a Poisson probability distribution that assumes foliage is randomly distributed. The term Plant Area Index (PAI) is adopted here since the entire plant and not just leaves are included in the photo-images. A comparison between the PAI of synthetic and actual hemisphericals can be made, even though the assumption of random distribution of foliage is not well suited for the clumped foliage at this coniferous site. Seasonal differences in PAI will need to be considered for an all-seasons model.

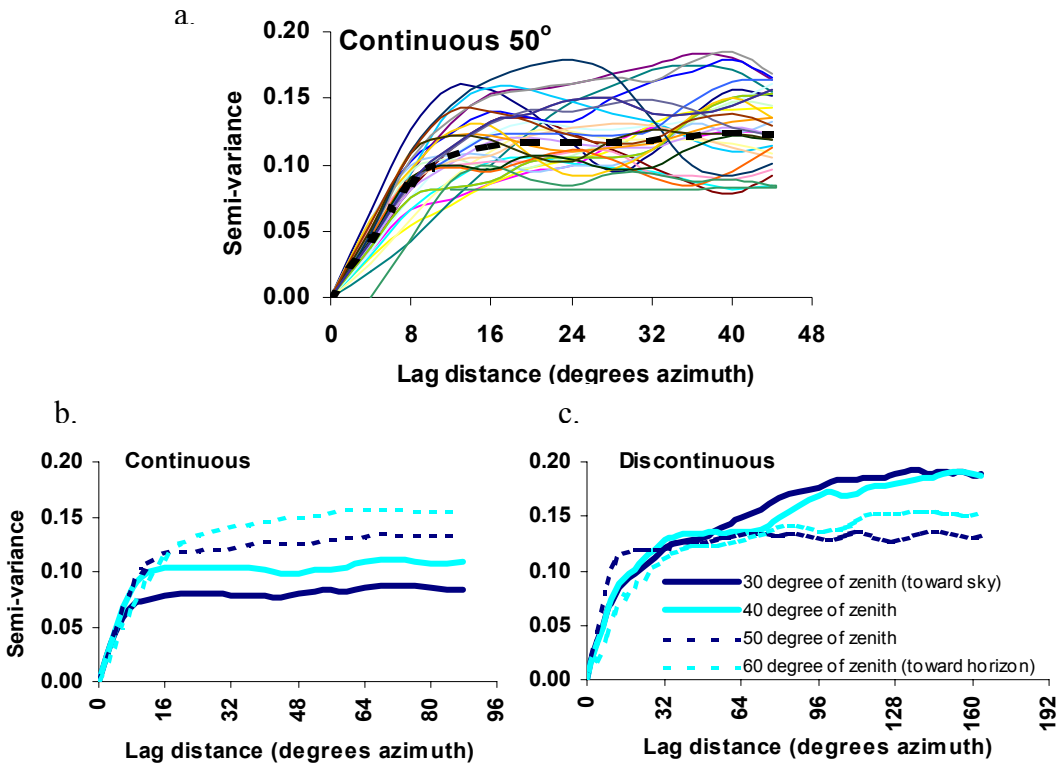

Figure 5. Variograms of a) individual hemispherical photo-images for 50° zenith with the mean shown as the heavy dashed line, b) mean variograms for a range of zeniths in the continuous canopy, and c) mean variograms for same range in the discontinuous canopy.

3-D Model Synthesis

Three-dimensional individual trees (Fig. 7) were developed using the detailed geometric measurements. The data were then input into the Onyx Tree Conifer software (Bosanac and Zanchi 2002) to generate the final geometric models for each individual tree in the LSOS. Modeling individual needles is possible, though too computationally intensive for rendering, so needles on each twig section were represented as replicated needle volumes. The synthetic trees were exported in ASCII facet format and a 3-D scene created with the Radiance ray-tracing software. Hemispherical views were generated by the ray tracing software for each location hemispherical photographs were taken. Equal area gap fractions for actual and synthetic hemispherical images were compared for cells in the interior of the plot for which specific tree dimensions (crown heights, crown widths, and DBH) were measured in the field (Fig. 8).

Gap Fraction Maps at Landscape Scale

Viewable gap fraction maps were generated for the landscape encompassed by the Fraser digital elevation model (DEM), a 10.6- by 13.8-km area at 30-m cell resolution, using software developed at Boston University (Liu and Woodcock 2002) in the Image Processing Workbench (IPW) (Frew 1990). The model, VGF (viewable gap fraction), is based on the geometric-optical (GO) bidirectional reflectance distribution function (BRDF) model (Li et al. 1995). VGF assumes a random (Poisson) distribution of tree locations within map units of a specified percent cover. Spatial maps of terrain slope, terrain aspect, view zenith angle, view azimuth angle, tree species, and percent cover were required input. Crown ellipticity (b/R=vertical crown radius / horizontal

crown radius) for each tree species was also required. The geometric consequences of terrain on viewable gap fractions are illustrated in Figure 9. A 30-m resolution viewable gap fraction map (Fig. 10) was derived assuming a 45% cover of lodgepole pine, view and zenith angles of 30°, and median crown ellipticity measured at the Fraser LSOS of 2.75. The use of a singular tree species and percent cover isolates for the influence of terrain in this demonstration.

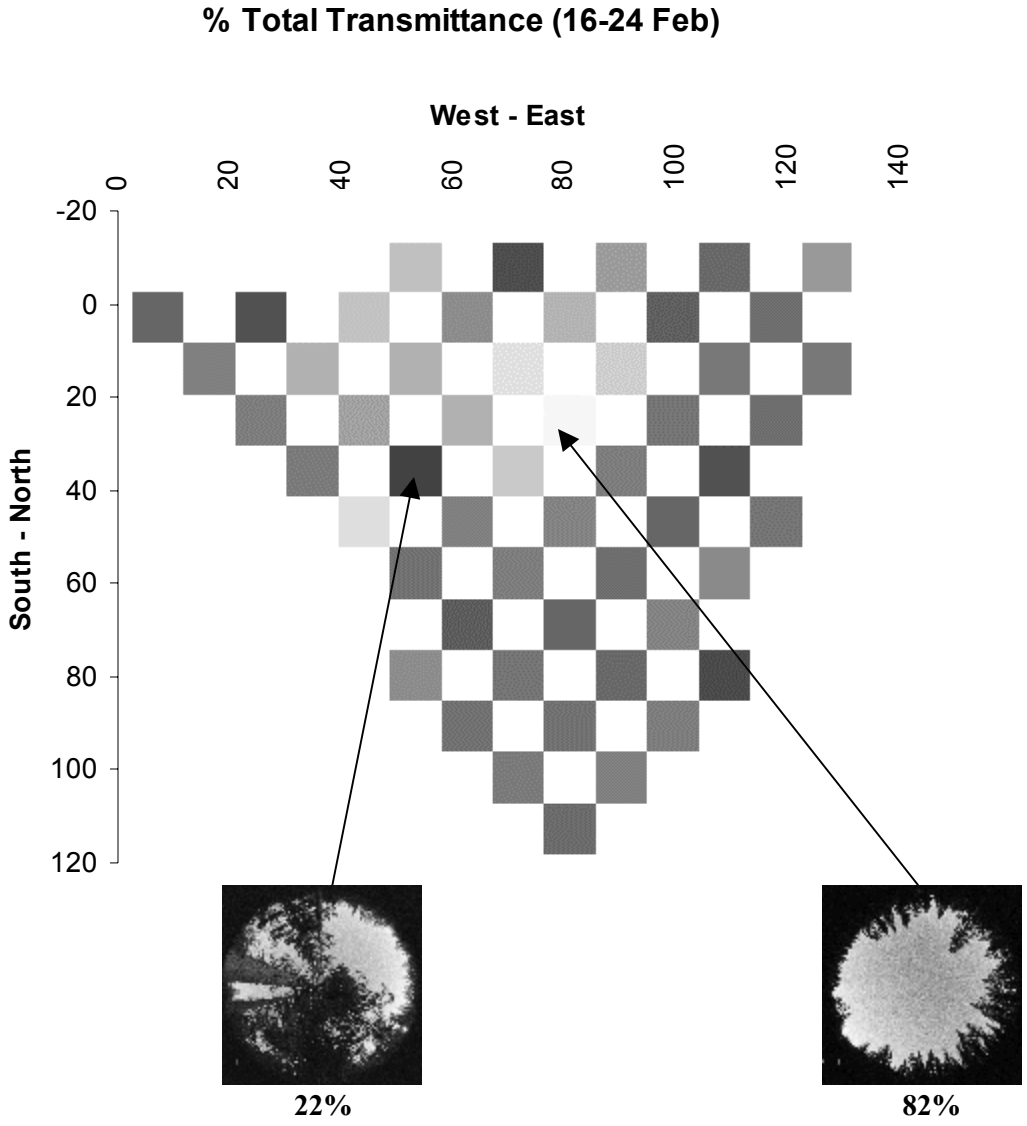

Figure 6. Spatial map of total daily transmittance for average sky conditions. The total transmittance varied from 82 to 22 percent of the above canopy total solar radiation. Maps can also be generated for PAI, and diffuse and direct components of solar radiation.

RESULTS AND DISCUSSION

Gap Fraction Distributions

The gap distributions for continuous and discontinuous canopy differ. Continuous canopy distributions have higher maximum frequencies (height on y-axis Fig. 4) occurring at lower gap fractions (length along x-axis, Fig. 4). Gap fraction distributions between zeniths of 0^{o} and 30^{o} represent sky and canopy tops that diffuse radiation penetrates. In this skyward 30^{o}, gap fractions are lower for continuous canopy (Fig. 4a) with the most frequent values around 0.5 to 0.6 compared to 0.9 in the discontinuous canopy (Fig. 4b). The 30^{o} to 60^{o} zenith range represents canopy that most of the direct midday radiation penetrates. The gap fractions in this mid range are lower for the continuous canopy, with the most frequent values around 0.4 to 0.5, compared to 0.5 and 0.7 in the discontinuous canopy. The 60^{o} to 90^{o} zeniths are closest to the horizon, where gaps are less frequent due to the long path length through the canopy and the effect of the lower portions of the canopy, tree trunks, shrubs and local terrain. The gap fractions are again lower for the continuous canopy with the most prevalent values in the 0.0 to 0.3 range compared to 0.0 to 0.4 in the discontinuous. The gap fraction distributions for continuous settings clearly show a decrease in the peak gap fraction frequency, as zenith angle increases through canopy tops, mid-canopy and lower canopy (Fig. 4a).

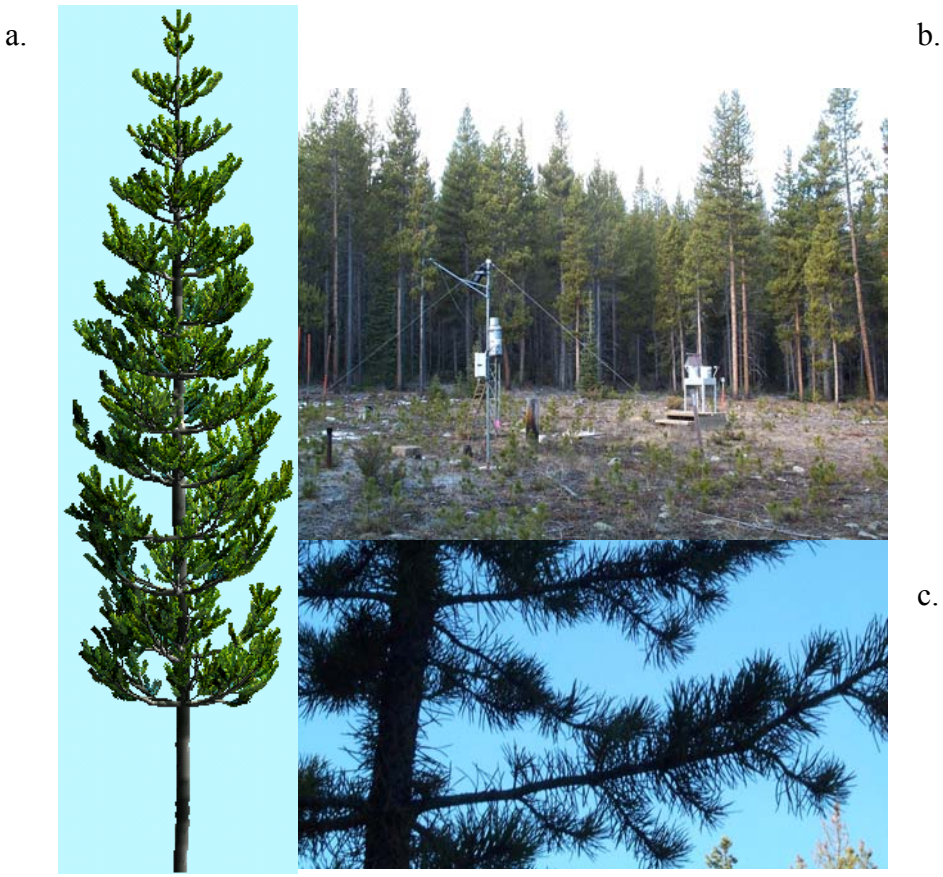

Figure 7. a) 3-D synthetic lodgepole pine, b) lower branches are lost from the lower part of the tree stems (top right) in older trees particularly when in dense stands, c) young trees have needles and branches on the main stem.

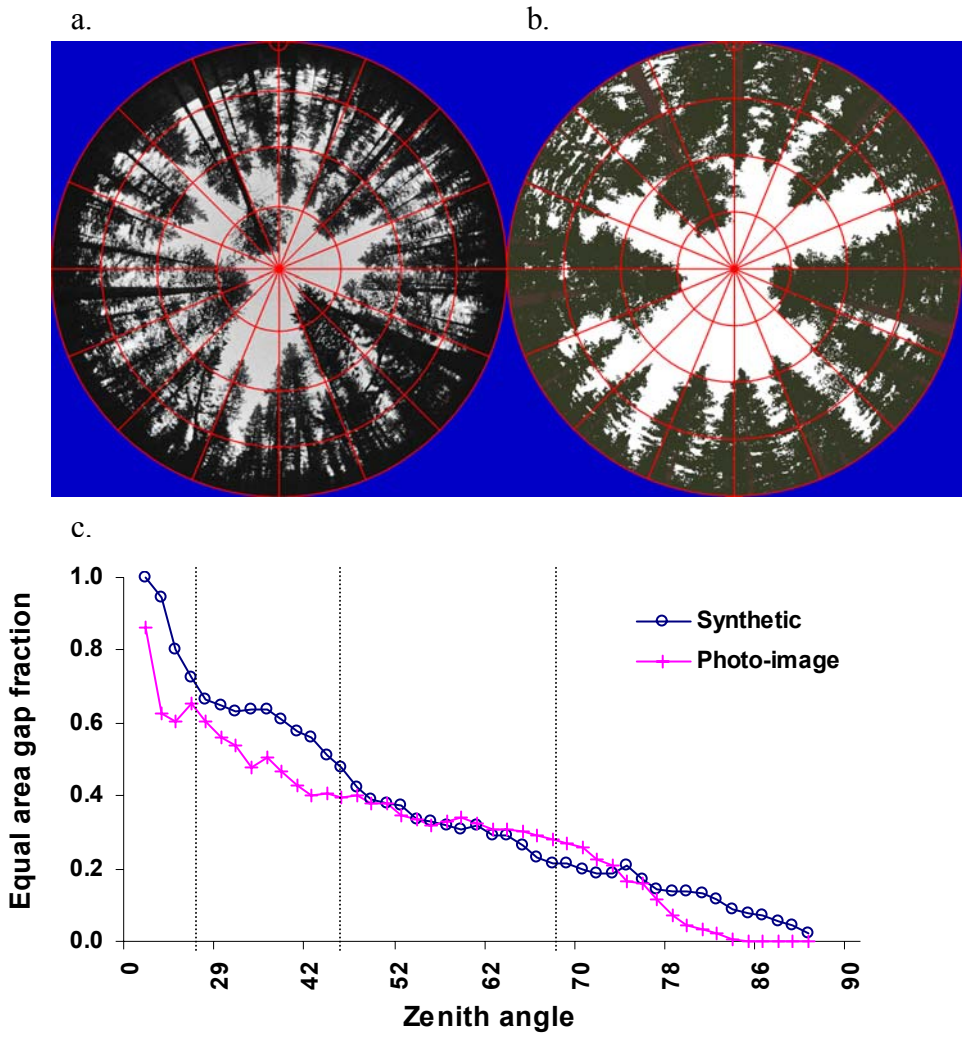

Figure 8. a) The hemispherical photo-image with a mask at 90° zenith and Nikkor lens projection grid at 0°, 22.5°, 45.0°, 67.5°, and 90°, b) the synthetic image with polar projection grid, and c) equal area gap fractions with corresponding vertical grid lines.

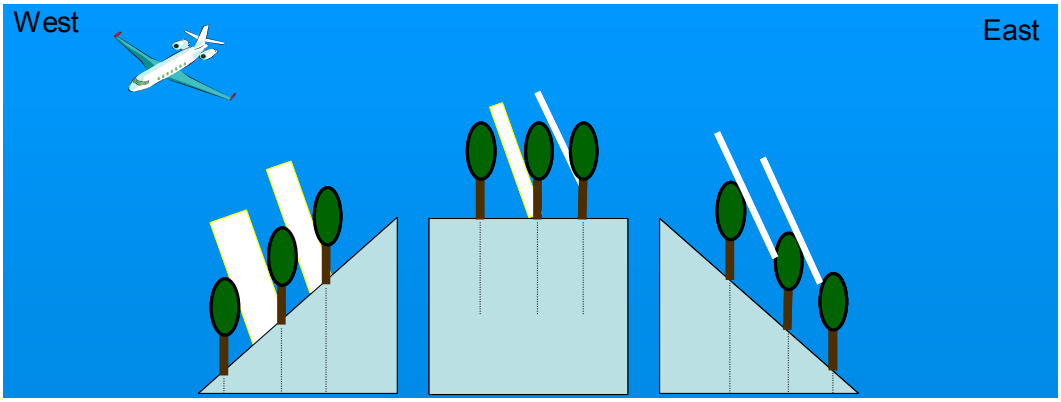

Figure 9. Schematic of viewable gap fraction dependency on slope and aspect.

Gap Fraction Correlation Lengths

The correlation length varies from image to image (Fig. 5a). Mean variograms for the continuous site (Fig. 5b) show that average correlation length increases from (approximately) 10^o to 20^o azimuth, between the 30^o and 60^o zeniths. [Azimuth degrees increase in arc-length as zenith angle increases; therefore, if converted to units of arc-length, the trend of increasing lag length would persist.] The average variograms for the discontinuous portion of the plot (Fig. 5c) are less consistent, but clearly show that average correlation lengths are longer and maximum variances higher than in the continuous canopy. Further exploration will be required to fully explain what the differences in variograms mean in terms of differences between discontinuous and continuous canopy structure. The longer correlation lengths in the discontinuous canopy may represent larger gaps. Increasing correlation length at higher zenith angles in the continuous portion of the site may represent increasingly contiguous canopy. The trend in variograms (Fig. 5b and 5c) as zenith angle increases suggests that covariance between gap fractions in adjacent zeniths may be higher for the continuous settings.

Canopy Transmittance and PAI

Total daily transmittance for 16-24 February varies from 22% to 82% for the hemispherical photograph locations (Fig. 6). Transmittances are generally lower in the continuous portion of the plot and higher in the discontinuous. Unexpectedly, the photograph with 22% transmittance is in the discontinuous portion of the plot where a large tree crown blocked the majority of the sun path across the south quadrant of the hemisphere. The photo-image with the highest transmittance is toward the north edge of the small opening. The diffuse and direct components of solar radiation transmittance (not shown) vary from 24% to 81% and from 9% to 83%, respectively. The PAI varies between 0.31 and 1.6. Spatial variation in radiation with zenith angle, at north and south edges of the central opening, have been examined with GLA (Melloh et al. 2002) and illustrates how light environment varies with sun zenith angle and for positions within a gap or gap edge. A study comparing radiation measurements at the LSOS with GLA radiation estimates is in progress (Hardy et al. in progress).

Synthetic and Actual Hemispherical Image Comparisons

Comparing tree locations along the north-south axis indicates the photo-image was rotated a few degrees east of north compared to the synthetic image (Fig. 8). This was due to the approximate north alignment of the camera and did not impact gap fraction zenith relationships presented here, since azimuthal differences were ignored. The synthetic image has more gap fraction near the horizon and this is due, in part, to a nearby ridge crossing the northeast quadrant of the photo-image (Fig. 8a) that is not accounted for in the synthetic image. The synthetic image also did not include shrubs that were ignored in the tree survey, or unmapped trees outside the border of the plot, though these affect the photo-image. This photo-image was taken at an interior location (Fig. 2, photograph 41). Inaccuracies due to unmapped trees bordering the plot will amplify for synthetic images derived for locations closer to the plot edge. The gap fractions are similar in the 45^o to 67.5^o range, though the synthetic canopy appears more spatially coherent while the photo-image canopy appears more disperse. Most of the disparity occurs from 0^o to 45^o with the synthetic image having consistently more gap area. The tree crowns appear more robust in the synthetic image; however, crown top heights of synthesized trees appear lower than actual heights. Inaccurately measured tree heights due to standing too close to the trees and not actually viewing the tops may be the cause.

Improvements in the 3-D representation can be made, but it is also clear that some differences will persist because of practical limitations of field data and model representations. Fine-tuning efforts will likely be limited to those that can be expected to have an impact on the IR model results. The 3-D representation could be improved by including the northeast ridge in the synthetic image, fine-tuning tree heights using additional field measurements or LIDAR, and including a buffer of trees beyond the site boundaries using LIDAR or orthophotographs.

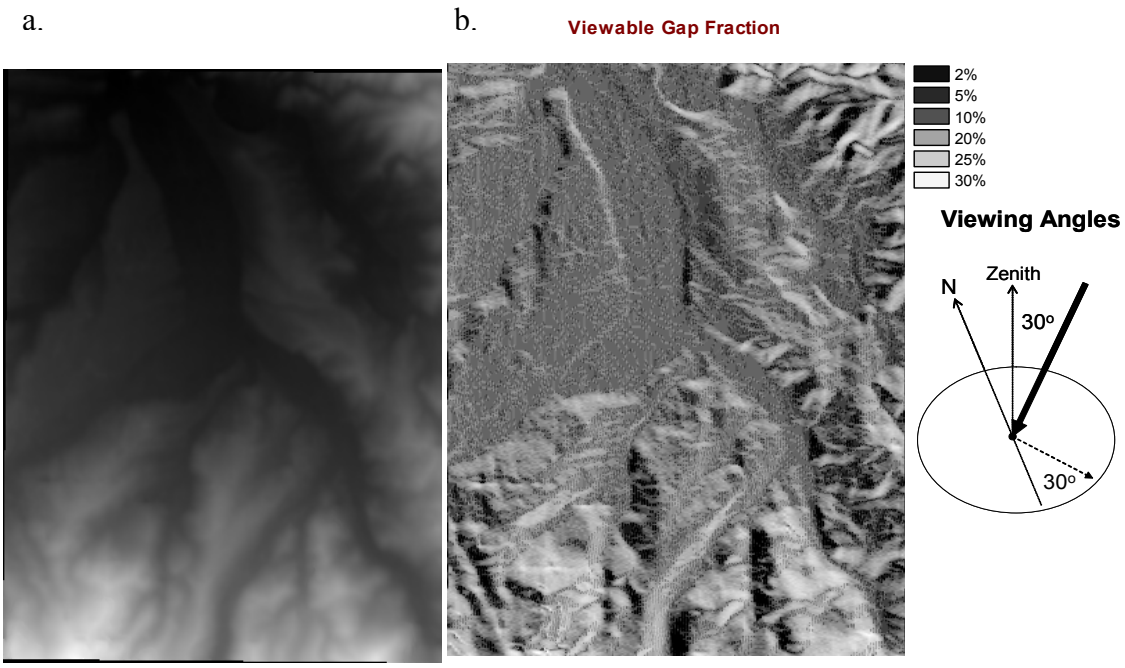

Figure 10. a) a 30-m resolution digital elevation model of the Fraser, Colorado topographic quadrangle, b) a viewable gap fraction map assuming constant tree ellipticity (b/R=2.75) and tree density (45% cover). Viewable gap fraction varied from 30% on facing slopes to 2% on opposed slopes.

Differences between the actual and synthetic trees will persist because while each tree is unique a limited set of shape parameters will be used to generate the trees. Older trees, for example, tend to loose foliage lower on the main stems (Fig. 7b) but younger trees still have this foliage (Fig. 7c), and trees situated in preferred sun-moisture-nutrient environments will be more robust. The simplification of needle groups into replicated needle volumes may change the small scale spatial variation of gaps within the tree crowns, but how important this is to IR modeling is uncertain.

Viewable Gap Fraction in Terrain

The relevance of terrain in determining viewable gap fraction was illustrated (Fig. 9). When viewed from the west during mid-day, viewable gaps on west facing slopes are large and mostly sunlit, gaps on flat slopes are small and mostly shaded, and gaps on east facing slopes are not viewable. When viewed from the east (not illustrated), large shaded gaps are viewable on east facing slopes, small and mostly shaded gaps are viewable on flat slopes and no gaps are viewable on west facing slopes.

The viewable gap fraction results (Fig. 10) for the specified viewing geometry, identified locations in the landscape where snow (or soil) could be seen through gaps, or obscured by canopy. The canopy was a hypothetical uniform cover consisting of a random (Poisson) distribution of tree locations, and with identical tree crown ellipticities throughout the entire DEM. Sunlit and shaded gaps were combined in this example, but will be separated in a future model version.

The impact of assumptions made in generating the viewable gap fraction maps that may be tested in the CLPX study area include: 1) do VGF's random tree distributions sufficiently represent the distribution of gap fractions in actual forest patches, 2) do VGF's uniform species and percent cover within a map unit satisfactorily represent actual forests with subdominant crowns and under story, and 3) how might VGF be modified to characterize gap fractions along forest edges.

SUMMARY AND CONCLUSION

Several characteristics of the Fraser LSOS lodgepole pine canopy were derived from hemispherical photographs. A comparison of these characteristics with those derived from synthetic hemispherical photographs provides a validation approach for a 3-D synthetic canopy model. The characteristics include gap fraction distributions, gap fraction variograms, subcanopy radiation environment, and PAI. The gap fraction distributions for continuous and discontinuous canopy settings differ. The continuous canopy has more peaked distributions and the discontinuous canopy has broader, flatter peaks. This reflects the greater canopy heterogeneity in the discontinuous settings. There is a regular transition in gap fraction distribution shape and peak position with progression of zenith angle range (sky, mid-canopy, and near horizon). Mean correlation lengths increase from 10^o to 20^o azimuth between the 30^o and 60^o zenith angles, in the gap fraction variograms for continuous settings, and the variogram sills (maximum variances) increase regularly with increased zenith angle. The averaged variograms for the discontinuous portion of the plot are less consistent, but clearly show longer averaged correlation lengths and higher maximum variances than in the continuous settings. GLA estimates of daily diffuse, direct and total solar radiation transmittance can be compared for specified sky conditions and calendar dates for each hemispherical location. PAI estimates from actual hemisphericals and synthetic ones should also be similar.

Preliminary progress in comparing actual and synthesized hemispherical photographs revealed some differences. Improvements needed include: 1) resolving why some tree heights appear taller in the photo-images than the synthetic hemispherical, 2) including trees from outside the gridded plot in the 3-D model, and 3) correcting for local terrain in the northeast quadrant of the view.

Validation studies for VGF will center on observing gap fraction statistics at "ground truth" forest sites to assess how well VGF estimates observed gap fraction probabilities. These comparisons will shed light on the impacts of subdominant crowns, understory and assumed random distributions of trees on the prediction of viewable gap fractions in the Fraser LSOS and other CLPX study areas.

ACKNOWLEDGEMENTS

The authors thank Kelly Elder, Marian Lathrop and Laurie Porth of the US Forest Service for assistance before and during our stay at the Fraser Experimental Forest. Funding was provided by Army AT24 project SS010 – All season heterogeneous 3-D discontinuous canopy model.

REFERENCES

Bosanac B, Zanchi P. 2002. Onyx Tree Conifer User's Manual. Version 5.1. Onyx Computing Inc., 10 Avon Street, Cambridge, MA .

Cline D, Elder K, Davis R, Hardy J, Liston G, Parsons M. 2002. The NASA Cold Land Processes Experiment (CLPX-2002). Microwave Remote Sensing of the Atmosphere and Environment, Proceedings of the Spie Vol. 4894, 24025 October 2002, Hangzhou, China, p. 361-372.

Fraser GW, Canham CD, Lertzman KP. 1999. Gap Light Analyzer (GLA), Version 2.0: Imaging software to extract canopy structure and gap light transmission indices from true-color fisheye photographs, Users manual and program documentation. Simon Fraser University, Burnaby, British Columbia, and the Institute of Ecosystem Studies, Millbrook, New York; 36 pp.

Frew JE. 1990. *The Image Processing Workbench*. PhD Dissertation, University of California, Santa Barbara.

Hardy J, Melloh R, Koenig G, Pomeroy JW, Marks D, Link T. In progress. Solar radiation transmission through conifer canopies. Presented at the IUGG, Sapporo, Japan, 3-11 July 2003; Workshop: JWH01 Snow Processes: representation in atmospheric and hydrological models.

Hutchinson BA, Matt DR, McMillen RT. 1980. Effects of sky brightness distribution upon penetration of diffuse radiation through canopy gaps in a deciduous forest. *Agriculture and Forest Meteorology* **22**:137-147.

Kimes DS, Kirchner JA. 1982. Radiative transfer model for heterogeneous 3-D scenes, *Applied Optics*, **22**:4119-4129.

Koenig G, Ballard J, Hardy J, Melloh R and Smith J. 2000. Heterogeneous 3-dimensional discontinuous canopy model, unpublished CRREL AT24 proposal.

Li X, Strahler AH, Woodcock CE. 1995. A hybrid geometric optical-radiative transfer approach for modelling albedo and directional reflectance of discontinuous canopies, IEEE Trans. on *Geoscience and Remote Sensing* **33**(2):466-480.

Liu J, Woodcock CE. 2002 (unpublished). Estimating viewable gap fractions in forest canopies: Implications for remote monitoring of snow and forest. Department of Geography, Boston University.

Melloh R, Woodcock C, Liu J, Hardy J, Koenig G. 2002. Viewable gap fractions in forests at the landscape and stand scale near Fraser, Colorado. Abstract. Presented at the Fall Meeting of the American Geophysical Union, San Francisco, California December 2002.

Webster R, Oliver MA. 2001. *Geostatistics for Environmental Scientists*. John Wiley and Sons, New York.

Wells JM, Norman JM. 1991. Instrument for indirect measurement of canopy architecture. *Agronomy Journal* **83**:818-825.